BL20B2
Medical and Imaging I

1. Introduction

BL20B2 is a medium-length beamline with a bending magnet source. It is composed of an optics hutch (OH), upstream experimental hutch 1 (EH1) located 42 m from the source, and downstream experimental hutches 2 (EH2) and 3 (EH3) located more than 200 m from the source. EH1 is located in the storage building, whereas EH2 and EH3 are located in the Medium-Length Beamline Facility.

BL20B2 is mainly used for X-ray imaging experiments such as X-ray micro-tomography (X-ray micro-CT) and real-time radiography. In EH1, high-spatial-resolution and ultrafast imaging experiments, which require a high photon flux density, are performed. In comparison, X-ray imaging experiments with a wide field of view (wFOV) are performed in EH2 and EH3 using an X-ray beam with a large cross section. In addition, X-ray phase-contrast imaging based on the high spatial coherence of the beam generated over a large propagation distance from the source is also performed. Furthermore, the almost parallel beam is applicable to the evaluation of X-ray optical devices and X-ray detectors. A standard double-crystal monochromator (DCM) and double-multilayer monochromators (DMMs) for X-ray energies of 40 and 110 keV are available as beamline monochromators [1]. As one of the activities in FY2024, a wFOV X-ray imaging detector was developed and applied to multiscale X-ray imaging.

2. Development of wFOV X-ray imaging detector

At BL20B2, it is possible to use wide X-ray beams in EH2 and EH3, as mentioned above. To perform wFOV X-ray micro-imaging using the wide X-ray beams, a dedicated wFOV X-ray imaging detector was developed. So far, X-ray imaging detectors with a field of view (FOV) of up to 50 mm have been used by employing a tandem lens system [2]. In developing the new wFOV X-ray imaging detector, securing an FOV of more than 90 mm, which is approximately twice the FOV of the conventional detector, was set as a goal. In wFOV X-ray micro-imaging, high-energy X-rays are expected to be used from the perspective of X-ray transmission for measuring relatively large objects. Therefore, the design was such that the detector could also be used for high-energy X-ray micro-imaging. Specifically, as with conventional X-ray imaging detectors, a visible-light conversion-type imaging system was employed, and the visible-light image converted by the scintillator was imaged onto a CMOS camera using a single lens. In this design, a lens with a large working distance was employed to allow the optical axis of visible light to be bent by 90 degrees from that of the X-ray, preventing high-energy X-rays passing through the scintillator from entering the lens and CMOS camera. Moreover, a telecentric lens with a large aperture and 0.2x magnification was used as the single lens to achieve wFOV and distortion-free imaging. The scintillator was a LuAG:Ce^{+} single crystal with a size of 100 mm x 25 mm and a thickness of 0.5 mm. A 4K CMOS camera (ORCA Quest, Hamamatsu Photonics) was used to enable high-definition measurements. The interior of the developed X-ray imaging detector is shown in Fig. 1.

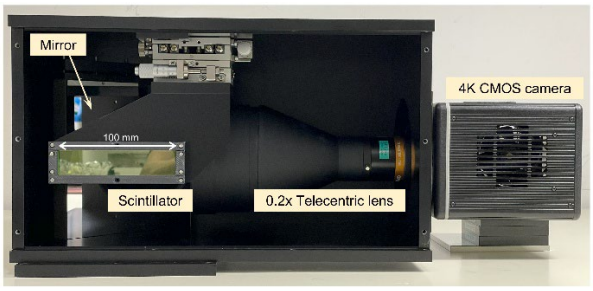

Fig. 1. Interior of wFOV X-ray imaging detector.

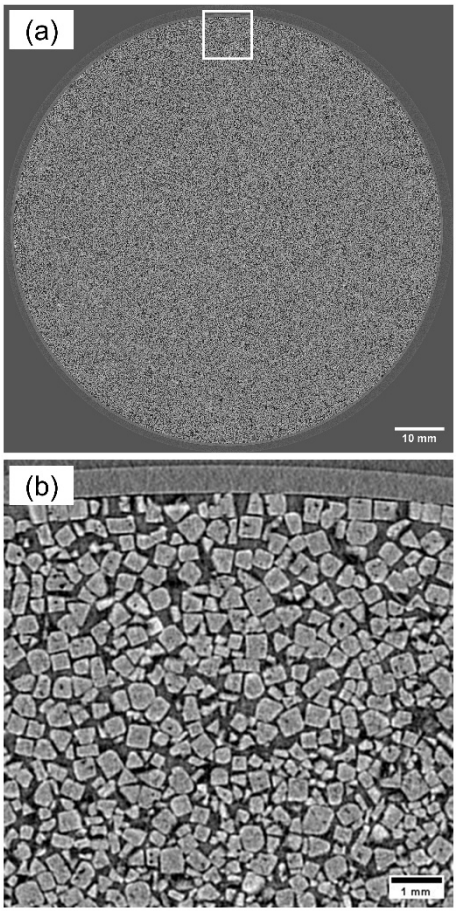

Fig. 2. (a) X-ray micro-CT image of sodium chloride particles measured with the developed wFOV X-ray imaging detector. (b) Magnified image of square region in (a).

To evaluate the developed wFOV X-ray imaging detector, especially in terms of image distortion in the effective FOV, the X-ray micro-CT imaging of sodium chloride particles spread out on a petri dish that fits exactly within the effective FOV was performed. The X-ray energy was 110 keV, and the propagation distance from the sample to the detector was set to 8 m. Then, the effective pixel size at the sample position was 22.08 μm, which was slightly smaller than the expected pixel size of 23 μm calculated from the magnification factor of the lens. This is because the X-ray transmission image was slightly magnified by the long propagation distance. The X-ray micro-CT image of the particles is shown in Fig. 2(a). In addition, the magnified image at the upper end is shown in Fig. 2(b). In the magnified image, the shape of the particles is clearly visualized; therefore, no significant image distortion was detected.

3. Application to multiscale X-ray imaging in macro to micro regions

Multi-scale X-ray imaging, which involves wFOV measurements using the developed wFOV X-ray imaging detector and localized high-resolution measurements for the region of interest based on the overview information obtained from the wFOV measurements, was demonstrated. The actual setup for the multiscale X-ray imaging is shown in Fig. 3. In this setup, a sample, high-resolution X-ray imaging detector, and wFOV X-ray imaging detector were arranged in this order, and it was possible to switch between high-resolution and wFOV measurements by moving the high-resolution detector in and out of the X-ray beam without removing the sample. Demonstrations of multiscale X-ray imaging were performed with the X-ray energies of both 40 and 110 keV.

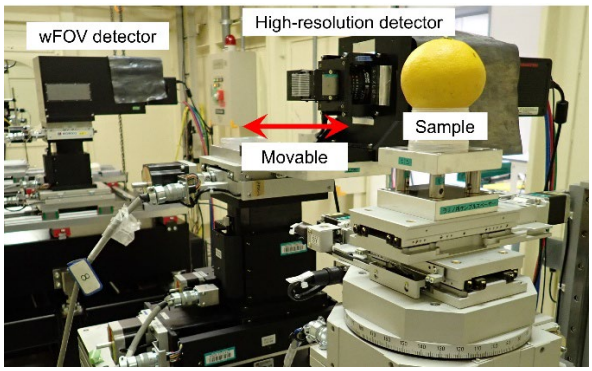

Fig. 3. Actual setup for X-ray multiscale X-ray micro-CT.

First, the multiscale X-ray micro-CT of a fruit (*Citrus tamurana*) was performed using 40 keV, with the intention of applying this measurement technique to organic materials such as biological samples composed mainly of light elements. In the wFOV measurement, the effective pixel size was 22.68 μm at the propagation distance of 2 m. In the high-resolution measurement, a visible-light conversion-type X-ray imaging detector with a tandem lens system was used. In this case, the effective pixel size was 1.26 μm. As well as the wFOV detector, a 4K CMOS camera (ORCA Fire, Hamamatsu Photonics) was used. Then, the effective FOV in the high-resolution imaging was 5.58 mm. The multiscale X-ray micro-CT images obtained at 40 keV are shown in Fig. 4. A circular region indicated in the wFOV image was measured with the high-resolution detector. While the whole internal structure of the sample could be seen in the wFOV image, fine structures such as cells and vessels could be visualized in the localized high-resolution image, as shown in the magnified image of the square region.

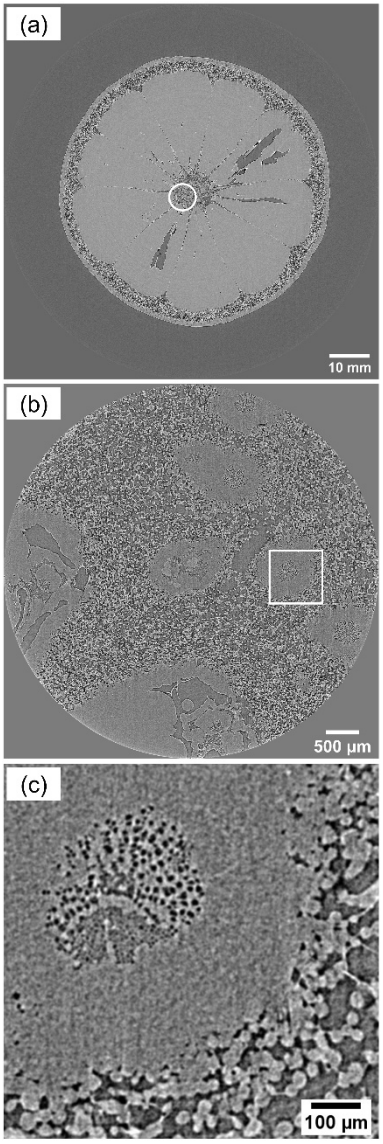

Fig. 4. Multiscale X-ray micro-CT images of *C. tamurana* measured with (a) wFOV and (b) localized high-resolution observations of circular region in (a). (c) Magnified image of square region in (b).

Next, the multiscale X-ray micro-CT of a nodule was performed using 110 keV with the intention of application to fossil samples. In the wFOV measurement, the propagation distance was set to 8 m. In the high-resolution measurement, the effective pixel size was 1.08 μm and the effective FOV was 4.98 mm when employing a 4K CMOS

camera (ORCA Lightning, Hamamatsu Photonics). The multiscale X-ray micro-CT images obtained at 110 keV are shown in Fig. 5. In the high-resolution measurement, a small fossil found in the wFOV image was observed. The detailed structure of the small fossil could be clearly visualized in three dimensions.

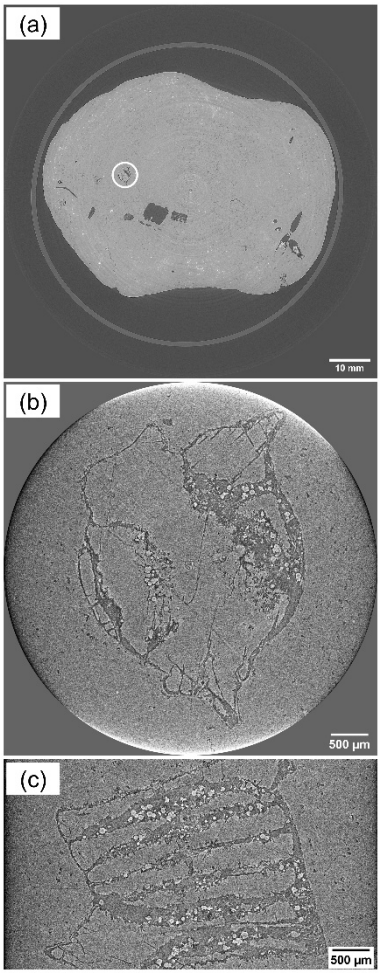

Fig. 5. Multiscale X-ray micro-CT images of a nodule sample measured with (a) wFOV and (b) localized high-resolution observations of circular region in (a). (c) Vertical sectional image obtained by high-resolution observation.

4. Conclusion

A wFOV X-ray imaging detector that matches the beam characteristics of BL20B2 was developed. It enabled high-definition X-ray micro-CT with an FOV of more than 90 mm, which was approximately twice the FOV of conventional measurements. In multiscale X-ray micro-CT using the developed X-ray imaging detector, it was demonstrated that it is possible to measure the whole structure of relatively large samples and its localized fine structure at the region of interest. Although only the results of multiscale X-ray micro-CT are shown, it is also possible to perform multiscale X-ray micro-laminography that is more effective for observing planar objects. As a future perspective, it is expected to be extended into multiscale X-ray imaging combined with higher resolution measurements available at EH1.

HOSHINO Masato and UESUGI Kentaro
Japan Synchrotron Radiation Research Institute

References:

[1] Koyama, T. Senba, Y. Yamazaki, H. Takeuchi, T. Tanaka, M. Shimizu, Y. Tsubota, K. Matsuzaki, Y. Kishimoto, H. Miura, T. Shimizu, S. Saito, T. Yumoto, H. Uesugi, K. Hoshino, M. Yamada, J. Osaka, T. Sugahara, M. Nariyama, N. Ishizawa, Y. Nakano, H. Saji, C. Nakajima, K. Motomura, K. Joti, Y. Yabashi, M. & Ohashi, H. (2022). *J. Synchrotron Rad.* **29**, 1265–1272.

[2] Hoshino, M. Uesugi, K. & Yagi, N. (2020). *J. Synchrotron Rad.* **27**, 934–940.